Structural Changes in Muscle Crossbridges Accompanying Force Generation

Keiko Hirose, Clara Franzini-Armstrong, Yale E. Goldman* and John M. Murray

Department of Cell and Developmental Biology, *Department of Physiology, and the Pennsylvania Muscle Institute, University of Pennsylvania, Philadelphia, Pennsylvania 19104-6058

Abstract. We have investigated the structure of the crossbridges in muscles rapidly frozen while relaxed, in rigor, and at various times after activation from rigor by flash photolysis of caged ATP. We used Fourier analysis of images of cross sections to obtain an average view of the muscle structure, and correspondence analysis to extract information about individual crossbridge shapes. The crossbridge structure changes dramatically between relaxed, rigor, and with time after ATP release. In relaxed muscle, most crossbridges are detached. In rigor, all are attached and have a characteristic asymmetric shape that shows strong left-handed curvature when viewed from the M-line towards the Z-line. Immediately after ATP release, before significant force has developed (20 ms) the homogeneous rigor population is replaced by a much more diverse collection of crossbridge shapes. Over the next few hundred milliseconds, the proportion of attached crossbridges changes little, but the distribution of the crossbridges among different structural classes continues to evolve. Some forms of attached crossbridge (presumably weakly attached) increase at early times when tension is low. The proportion of several other attached non-rigor crossbridge shapes increases in parallel with the development of active tension. The results lend strong support to models of muscle contraction that have attributed force generation to structural changes in attached crossbridges.

A complete understanding of a motile system would allow assignment of a specific structural configuration to each of the biochemical and mechanical intermediates in the cycle of the motor. In the case of skeletal muscle, energy-transducing crossbridges connecting the actin and myosin filaments constitute the motor. A goal that is more modest than complete understanding, but heretofore unrealized, is to observe the changes in structure of the actin and myosin molecules that occur between the initial attachment of crossbridges and their force-producing state. Direct visualization of these structural changes would provide enormous help toward explaining the mechanism of active filament sliding.

The structure of the rigor crossbridge (i.e., the actin–myosin link formed in the absence of ATP) has been well defined by electron microscopy both in isolated complexes in vitro, where all actomyosin pairs are identical (Taylor and Amos, 1981; Vibert and Craig, 1982; Toyoshima and Wakabayashi, 1985*a*,*b*; Milligan and Flicker, 1987; Flicker et al., 1991) and in muscle fibers, where the restricted choice of sites of origin and attachment on the myosin and actin impose variable structural distortions (Reedy and Reedy, 1985; Taylor et al., 1986, 1989). The study of actomyosin-based motility has recently been invigorated by the report of the atomic structure of myosin subfragment 1 (Rayment et al., 1993*b*), the motor domain of the protein, containing the actin and ATP binding sites. Combining this with the biochemical knowledge of the location of ATP and actin binding sites (Sutoh et al., 1986; Tokunaga et al., 1987; Yount et al., 1992), an atomic model of the actin filament (Holmes et al., 1990), and structural constraints derived from EM work (Milligan et al., 1990; Winkelmann et al., 1991), an atomic level model of the actomyosin interaction in the absence of ATP and detailed predictions of its changes during activity are now possible (Rayment et al., 1993*a*; Rayment and Holden, 1994).

Crossbridges in activated fibers have been more difficult to study, because of their dynamic nature, than rigor crossbridges. EM pictures of the isolated myosin–actin complex in the presence of ATP were obtained by rapidly stopping the motion using various approaches (Craig et al., 1985; Applegate and Flicker, 1987; Katayama, 1989; Frado and Craig, 1992; Funatsu et al., 1993; Pollard et al., 1993; Walker et al., 1994). Active crossbridges have also been trapped in situ, within the ordered structure of the muscle fiber, by using rapid freezing (Tsukita and Yano, 1985; Hirose and Wakabayashi, 1993; Hirose et al., 1993). Al-

Keiko Hirose's present address is MRC Laboratory of Molecular Biology, Hills Road, Cambridge CB2 2QH, England.

Address all correspondence to John M. Murray, Dept. of Cell and Developmental Biology, University of Pennsylvania, Philadelphia, PA 19104-6058. Tel.: (215) 898-3045. FAX: (215) 898-9871.

though not in agreement on details, these studies indicate differences in the overall appearance of populations of crossbridges in the presence and absence of ATP (but see Pollard et al., 1993) which are consistent with the changes from rigor to activation identified by x-ray diffraction studies (Huxley and Faruqi, 1983). However, matching these population differences to specific events of force generation and sliding has been difficult because during contraction many different biochemical and structural intermediates are simultaneously present.

Techniques that allow dissection of events in time, such as x-ray diffraction (Huxley and Faruqi, 1983) and ultra rapid freezing electron microscopy have the potential to identify the sequence of structural intermediates that underlie activation and development of force and sliding. X-ray diffraction has two major advantages over electron microscopy for this goal: it is capable of higher resolution than thin section EM, and x-ray diffraction spectra can be recorded in real time from intact muscle fibers. However, x-ray measurements are an average of all crossbridges. While a shift in this average can be detected, translating such shifts into actual changes of individual crossbridge configurations is not straightforward.

Electron microscopy circumvents some of the limitations of x-ray diffraction, albeit at the cost of lower resolution and the risk of introducing artifacts during sample preparation. Rapid freezing electron microscopy was combined with partially synchronized activation by photolysis of caged compounds to obtain time resolved images (Hirose et al., 1993; Lenart et al., 1993). These studies identified major variability of the shape and angle of the myosin heads during force development, which is established very early after photoliberation of ATP. However, sequential changes of the individual crossbridges from initial attachment to the force-producing states were difficult to detect because of the structural variability that was present even in the rapidly activated fibers.

In the present work we also used the rapid freezing technique on muscle fibers activated by photolysis of caged ATP. In this case we examined cross sections of the fibers to quantitate the mass and shape of the molecules in the radial and azimuthal directions around the thick filaments. By keeping track of the direction of view, we preserved the intrinsic handedness of the crossbridge structure, which is clearly seen in our results. We used correspondence analysis that has been so effective in identifying structural attributes of ribosomes and other non-crystalline biological structures (Harauz et al., 1988; Frank, 1990) to classify objectively individual crossbridges in the micrographs. This allowed several discrete crossbridge shapes to be distinguished, and their proportions as a function of time could be determined during activation. Comparison of these time courses with the development of tension provides constraints on the relationship of the various crossbridge shapes to the force generating event. Moreover the images obtained in rigor with known directionality could be compared with the structures expected from reconstruction of decorated thin filaments and the atomic map of the S1 head. Some of the results have been briefly reported in Hirose, K., J. M. Murray, C. Franzini-Armstrong, and Y. E. Goldman. 1993. *Biophys. J.* 64:27a.

Materials and Methods

Specimen Preparation and Microscopy

Preparation of Muscle Fibers and Rapid Freezing During Activation. Muscle fibers were chemically skinned and rapidly frozen during activation by photolysis of caged ATP as described previously (Hirose et al., 1993). Briefly, rabbit psoas muscle fibers were treated in a relaxing solution containing Triton X-100. Small bundles (1–5 fibers) were dissected and mounted on a freezing head (modified from a Cryo-press, Med-Vac Inc., St. Louis, MO). The fiber bundles were sequentially put into rigor, Ca^{2+} rigor, and finally Ca^{2+}-rigor solution with 10 mM caged ATP. They were frozen by allowing the freezing head to fall onto a metal block cooled by liquid helium. Caged ATP was photolysed by a laser pulse triggered at 20, 50, 80, or 300 ms before freezing. Control fibers were frozen in rigor and in relaxing solutions. An oscilloscope trace of the muscle fiber tension, along with the timing of release, flash, and smash, was recorded on diskette.

Electron Microscopy. The frozen fibers were freeze-substituted with 2–4% OsO_4 in acetone at −80°C for 2–4 d, warmed to room temperature, stained en block with 1% uranyl acetate in acetone, and then embedded in araldite. Thin sections were cut perpendicular to the fiber long axis and stained with potassium permanganate and lead citrate. The resultant cross-sectional images contain myofibrils with two opposite directions of view: from the M-line towards the Z-line or from the Z-line towards the M-line. The direction of view is difficult to determine simply by examining an image. For most of the images used for classifying the crossbridge shapes by correspondence analysis, the direction of view was determined by serial sectioning of the fibers over a length of ~2 μm (70 sections), including thin sections (20 nm) interspersed between thicker sections (40–70 nm), sufficient to be sure of including a length of the fiber extending from the middle of the thick filaments (M-line region) through and beyond the ends of the thick filaments. By taking low magnification micrographs of the thicker sections along this series at intervals of 5–10 sections, we could identify a fibril for which we had cut a complete M-line through Z-line sequence. We then used these low magnification micrographs to relocate this fibril and collect high magnification images of the thinner cross sections, taking care to control the orientation of the grid in the microscope and orientation of the film in the digitizer. By following this procedure, we knew the direction of view (e.g., from M-line towards Z-line) for each cross section and could therefore orient them all the same way. Micrographs for analysis were then obtained at a magnification of 24,400 from the sections of ~20-nm thickness. Off-axis focusing was used to minimize the electron dose to the sample. All images in Figs. 2–7 are displayed as if viewed looking from the M-line toward the Z-line.

Selection of Images and Digitization. The criteria for choosing areas to use for image processing were: (*a*) good freezing; (*b*) location well into the A-band (Regions close to the I-band were avoided because the thick filaments are thinner there.); (*c*) the plane of the section was as near as possible perpendicular to the filaments; (*d*) the filament lattice appeared well-ordered.

Image Processing

Fourier Filtration of Cross-sectional Images. All of the routine image processing and display operations utilized the Semper image processing software (Synoptics Ltd, Cambridge, UK). Electron micrographs of cross sections were selected for processing by examination of their optical diffraction patterns. Regions that appeared reasonably well ordered by optical diffraction were digitized on a raster of 25 μm (for image magnification of 24,400) using a microdensitometer (Model 1010G; Perkin-Elmer Corp., Norwalk, CT). Digitized images were corrected for lattice distortions using an unbending procedure similar to that described by Henderson et al. (1986). Briefly, a small well-ordered region within each micrograph was chosen as reference, and the cross-correlation map of this region with the rest of the image was calculated. Each peak of the cross-correlation map was assigned a lattice index, and its displacement from the ideal hexagonal lattice position was calculated. The resultant list of lattice displacements was used to warp (using a least-squares smoothed bicubic spline approximation [Henderson et al., 1986]) the original image onto a regular hexagonal lattice.

After scaling all of the images to zero mean density and equal variance, Fourier transforms were computed. For calculating [1,1]/[1,0] ratios, the density was summed within a 5 by 5 pixel box centered on the reciprocal

lattice points. The background density was estimated using the density values from a nearby area outside the peak, then subtracted from the sum. For calculating averaged density maps, the average phase residuals for each time-point were calculated as the sum of the absolute deviations of the symmetry related spots from their consensus value (which ideally is always 0 or π for p6 symmetry), divided by the total number of reflections. An average density map for each unbent image was computed by masking its Fourier transform to include only the reciprocal lattice points of the hexagonal lattice, enforcing p6 symmetry, and then calculating the inverse Fourier transform. A number of filtered images of different cross sections from each time point were averaged together to give the final density maps (21 for rigor, 7 for relaxed, and 11, 12, 13, 12 for 20, 50, 80, 300 ms after caged ATP photolysis, respectively).

Before computing difference maps between the different time points, we must scale the intensity of each image to make them comparable. Random variations in a number of factors (e.g., specimen thickness, degree of staining, microscope defocus and objective aperture settings, and film development) lead to artifactual variations in contrast. In addition, there are real variations between specimens that are not relevant to our concern with changes in crossbridge distribution. For example, rigor fibers are always better ordered than relaxed fibers, hence will retain a higher fraction of their true contrast after Fourier filtration. To get a reliable picture of the changes in the crossbridges, we have somehow to normalize the images to remove this irrelevant contrast variation. The most straightforward assumption, that the total scattering per unit cell remains constant during the activation process, turned out to be not applicable. If we tried to normalize the images by setting the mean value of each image to zero and making the total variance the same for all images, then the difference maps showed unreasonably large apparent variations in the density of the center of the thick filament backbone. Therefore we adopted an alternative normalization method, adjusting the total variance so that there was no significant change in the thick filament backbone among different time points. For simplicity, we scaled all of the density maps so that the average density within 6 nm from the center of the thick filament had equal value. This procedure leads to difference maps whose main features are compatible with the major changes expected on the basis of time resolved x-ray measurements of muscle during activation (Huxley and Faruqi, 1983), giving some confidence that the normalization is approximately correct.

Correspondence Analysis of Crossbridge Images. We developed a semiautomated method of locating individual crossbridges within a cross section and extracting each one into a separate small subimage. First, we constructed a list containing the locations of all possible nearest-neighbor actin–myosin (A-M) pairs (i.e., all potential crossbridge locations). This list was used to mark a graphic display of the original cross section, which allowed us to recognize and remove obvious defects (e.g., deposits of precipitated stain), and to add any potential crossbridge locations overlooked by the automated procedure. Apart from this editing, which removed less than 0.5% of the A-M pairs in any image, we used every A-M pair found within the successfully unbent region of each micrograph, without further selection. The corrected list of A-M pair locations was used to extract small subimages, regions just large enough and oriented appropriately to contain a single actin and one of its nearest-neighbor myosins, at each of these potential crossbridge locations. We brought all of the small subimages (each containing one A-M pair) from a single cross section into precisely the same orientation and magnification by three cycles of rotational and translational cross-correlation alignment and rescaling, using the global average of each cycle as the reference image for the next cycle. The entire set of aligned A-M pairs (~10,000 subimages, derived from 5–7 cross sections at each time point; a total of 70957 subimages from 35 cross sections) was normalized to constant mean and variance (Unser et al., 1989; Unser and Eden, 1990), with the variance chosen to ensure that there would be no negative pixels in the final data. This data set was then subjected to correspondence analysis (van Heel, 1984; Frank, 1990; Greenacre, 1993; Lebart, 1993) using software modified from a package written by and kindly supplied to us by J. P. Bretaudiere (Bretaudiere et al., 1981; Bretaudiere and Frank, 1986). We used a mask to exclude the region of the subimages containing most of the myosin filament backbones from the analysis, so that the variance components resolved by correspondence analysis would arise predominantly from differences in the crossbridges. The 16 largest eigenvectors of the matrix of pixel covariances were computed, of which the first 12 were used for classification as described below.

We determined the absolute hand of the crossbridge structure by serially sectioning each fiber as described above. For two cross section images from the 80-ms time point, and three from the 300-ms time point, we did not have a set of serial sections to use for determining orientation. To determine the correct orientation of these five cross sections we used the unequal distribution of crossbridge mass in the aligned and averaged images of A-M pairs.

Classification of Crossbridge Shapes. The 12 largest eigenvectors (components of variance) of the pixel covariance matrix were used to classify the set of A-M pair images from each time point separately. Every A-M pair image can be represented as a combination of the 12 eigenvectors in different proportions. The 12 proportions needed to represent a particular image denote its location in a 12-dimensional factor space. The first step of classification identified clusters (i.e., images having similar coordinates in the 12-dimensional factor space) based on four cycles of the dynamic clouds method (Diday, 1971; Frank, 1990). One cycle of this method consisted of five iterative partitionings around five centers. The initial five centers (seed objects) for each cycle were drawn at random from the entire set of A-M pair images. All images were individually grouped with the closest one (smallest Euclidean distance in factor space) of these five seed objects. Next, five new centers were computed as the centroids of each of the five clusters of assigned images. In the next iteration, all images were then reassigned to the closest one of the five new centers, and this process was iterated five times. Repetition of the entire cycle four times (starting each time with a fresh set of five randomly chosen seed objects) defines 625 ($= 5^4$) clusters, each cluster characterized by a unique combination of four centers, one center from each cycle. The 49 largest of these 625 clusters were retained, and the remainder were coalesced into a fiftieth cluster deemed, temporarily, unclassifiable.

This partitioning by dynamic clouds was then annealed by considering each image in turn, allowing it to migrate to a different cluster if the total intracluster variance would be thereby decreased, otherwise keeping it in its original cluster (van Heel, 1984). After each migration, the centroids of the donor and recipient cluster were updated. Sequential passes through the entire set of images were made until the clusters stabilized. At the end of this process, typically 10–15% of the images remained in cluster number 50, the unclassifiables. We formed an average image for each cluster by calculating the mean values, over all the images in the cluster, of the components of variance along each of the 12 identified variance axes. These average images are thus filtered in the sense that all components of variance other than those identified with the 12 largest eigenvectors have been eliminated. We denote these cluster averages as centroid images. For comparison, we also computed unfiltered average images by simply summing all of the A-M pairs belonging to a cluster. As expected, since the centroid images contain all the major variance components, the centroid image and the unfiltered average image were very similar.

When we examined the centroid images of the 49 stable clusters, identified as described above, we found that many of them differed in ways that were either insignificant or irrelevant for our purpose of classifying crossbridge shapes. Therefore, the 49 stable clusters were further aggregated by manually assigning them to one of 16 classes on the basis of the appearance of the crossbridge in the centroid image of each cluster. In other words, by ignoring differences outside the region of the crossbridge (see Results), we collapsed the 49 objectively obtained clusters down into a set of 16 classes that were more meaningful for our purposes. Hierarchical ascendant classification using Ward's criterion (Ward, 1963) produced a dendrogram for aggregation of the 49 clusters that was quite similar to the manual assignment. Each time point produced an essentially identical repertoire of 16 classes. The proportion of images falling into each of the 16 classes was determined for each time point, and is given in Results. Centroid images and unfiltered averages were also computed for these final 16 classes. As for the 49 objectively obtained clusters, the centroid images and the unfiltered averages were similar for each of the 16 aggregated classes.

Validation of Correspondence Analysis and Classification. We carried out several control procedures to validate the correspondence analysis and subsequent classification. In the first control, we checked that our methods could correctly retrieve a set of known structures from noisy data. We constructed a test data set by embedding a large number of model crossbridge images of 16 different types in fields of random noise having the same spectral distribution as the noise in our real data. The signal/noise ratio in the test images was made much worse than in our actual data, and sufficiently low that the test images were essentially invisible after embedding in the noise. Correspondence analysis followed by classification using the dynamic clouds technique with subsequent annealing was used to produce a partitioning into 49 clusters as described above. These 49 clusters were then aggregated by hierarchical ascendant classification using Ward's criterion into larger clusters. There is no general rigorous method of determining

how many distinct classes "exist" within a set of data (Mezzich and Solomon, 1980), so external criteria must be applied to make this decision. However, some statistical measures have been developed to serve as a guide. Using both the Calinski-Harabasz (1974) and the modified Hubert (Hubert and Arabie, 1985; Dubes, 1987) criteria, 16 classes were retrieved from the hierarchical ascendant classification. These 16 matched the input test images quite well. Thus the software acting on realistic data successfully retrieves only the structures known to be present.

In a second control, we simply repeated the classification of our real data using a different set of random seed objects as initial centers. The 16 classes formed were virtually identical to those formed previously, and the distribution between classes for each time point agreed to within a few percent.

In a third control procedure we carried out correspondence analysis and classification independently on data from each time point, instead of lumping all time points together for the eigenvector analysis. The sets of eigenvectors identified for the different time points were all different (they could all be recognized as alternative choices of coordinate axes in factor spaces with similar strong variance components), but the set of reconstituted centroid images from the final groups were essentially identical among all the time points. In other words, the same repertoire of crossbridge shapes was identified at each time point, even though a different set of eigenvectors was employed in each case. This gives very strong confirmation that the different classes of crossbridge shapes that we have identified represent real structural differences present in the original data.

Results

Rapid Freezing of Activated Muscles

Skinned fibers from rabbit psoas muscle were rapidly frozen while either relaxed, in rigor, or at various times after activation from rigor by flash photolysis of caged ATP. We searched for structural changes accompanying activation by analyzing electron micrographs of cross sections of fibers. Fig. 1 shows a low magnification view of a cross section and a typical tension record. The edge of the fiber, the surface which made direct contact with the liquid helium cooled freezing block, is visible at the top right of the figure. It is apparent from the images (and from their Fourier trans-

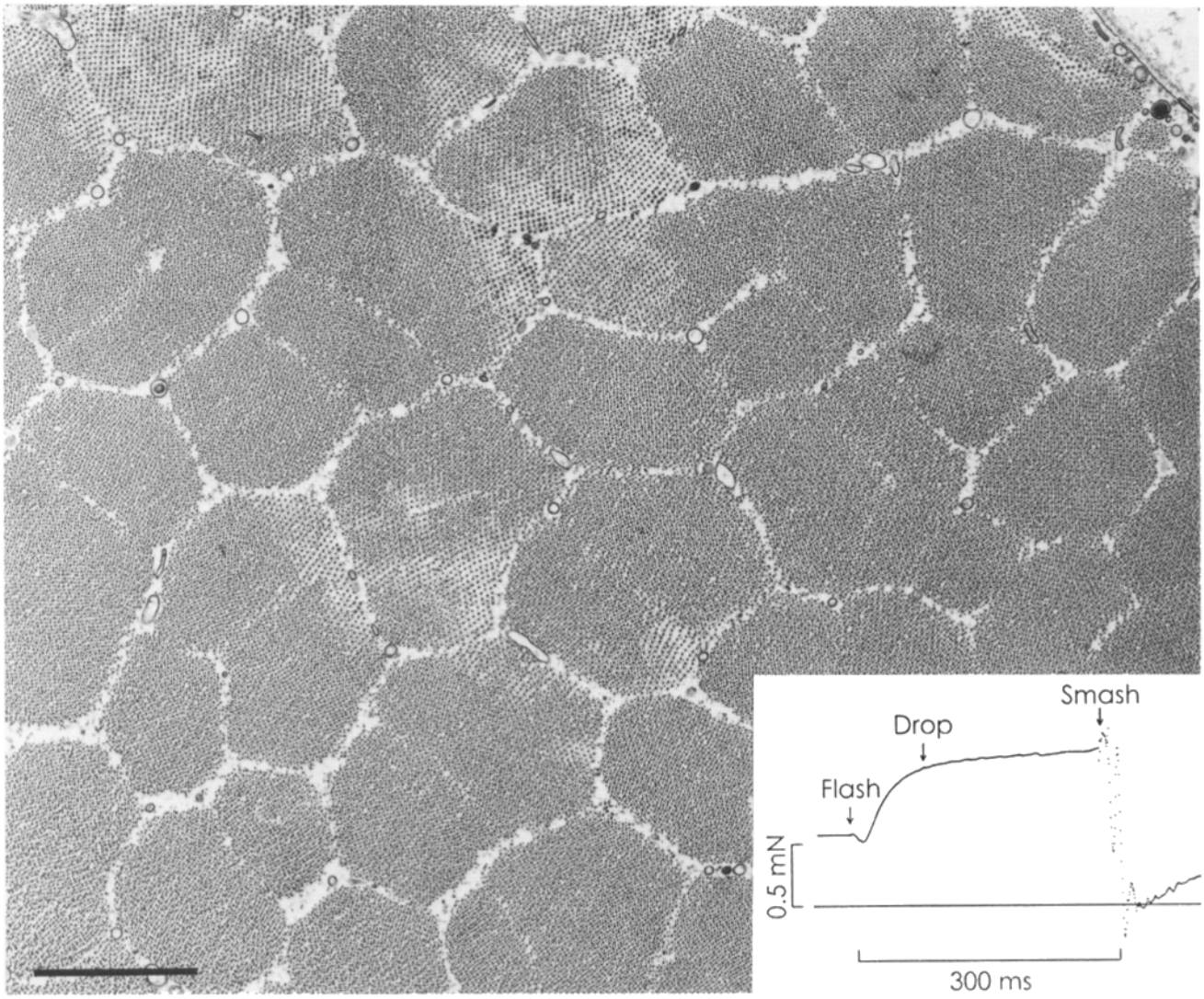

Figure 1. Low magnification electron micrograph of a cross section of a muscle fiber frozen at 50 ms after ATP release and prepared as described in Materials and Methods. The surface that made contact with the freezing block is at the top right corner. The region of good structural preservation extends through approximately two-thirds of the area shown. At the lower left corner some freezing damage is manifest as breaks and irregularities in the filament lattice. The inset shows a typical tension record for another fiber that was frozen 300 ms after ATP release. Photolysis of caged ATP occurs at the time indicated by *Flash*. The plunger holding the fiber and tension transducer falls toward a liquid helium cooled block (*Drop*) until contact occurs at *Smash*. Bar, 1 μm.

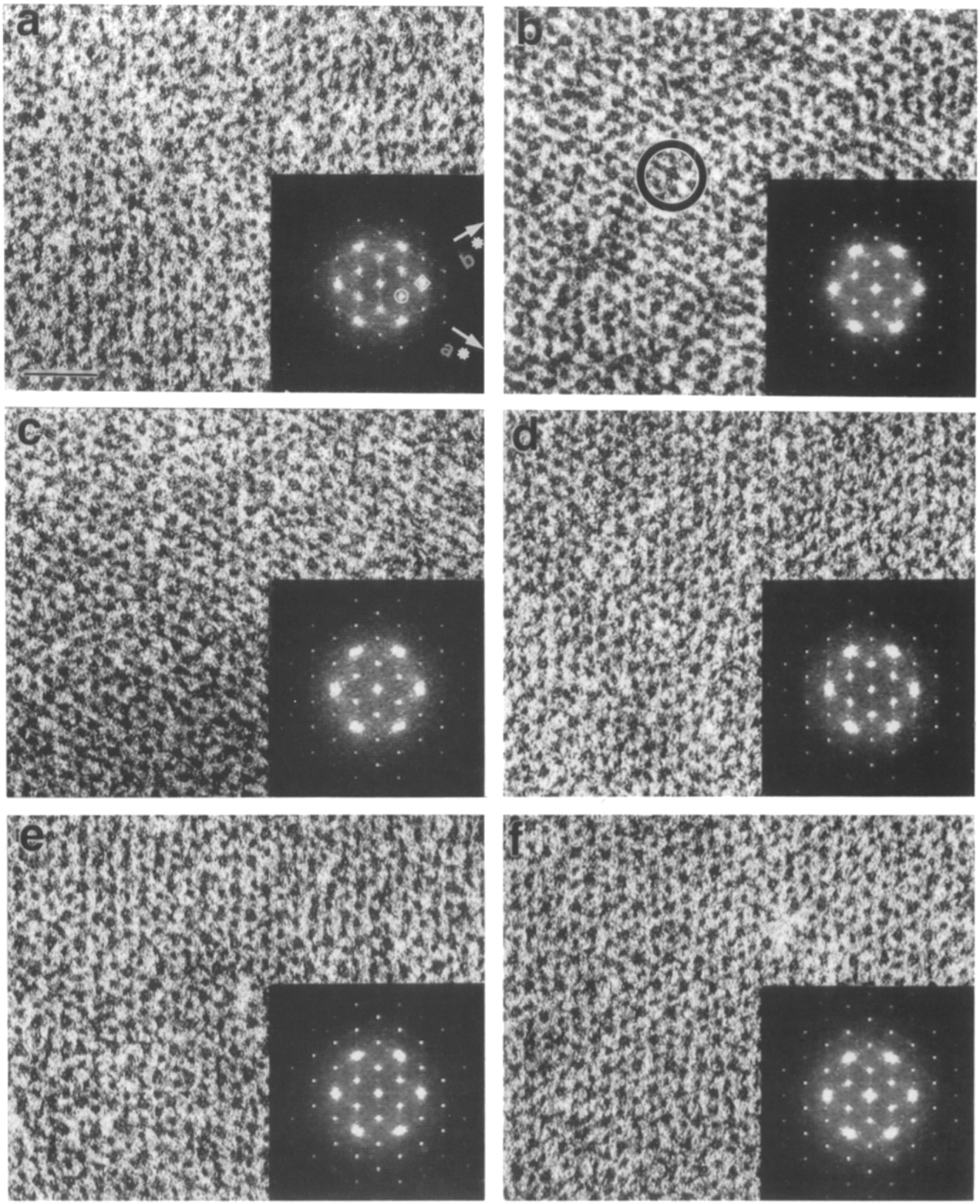

Figure 2. Images and power spectra of cross sections of fibers frozen while relaxed, in rigor, and at various times after release of ATP by flash photolysis. The images have been "unbent" as described in Materials and Methods. The power spectra are sums derived from 7–21 individual images. All images and power spectra are in the same orientation. (*a*) Relaxed, the arrows indicate the directions of the a^* and b^* axes; the small white circle and diamond in the power spectrum enclose a [1,0] and a [1,1] spot, respectively; (*b*) rigor, the circle in the image encloses a central thick filament surrounded by six thin filaments; (*c*) 20 ms; (*d*) 50 ms; (*e*) 80 ms; (*f*) 300 ms. Bar, 100 nm.

forms, see below) that the myofibrils have not been compressed, nor is there any sign of freezing damage for a depth of more than 5 μm from the surface. All of the micrographs we have analyzed are images of cross sections cut from regions of well-preserved structure near the edge of fibers such as this one.

Higher magnification views of cross sections of fibers that were frozen while relaxed, in rigor, and at 20, 50, 80, and 300 ms after release of ATP are shown in Fig. 2. In overall appearance the fibers are clearly different. Particularly when comparing rigor and relaxed, the apparent size of the actin filaments differs noticeably. In relaxed fibers, the actin filaments appear small and are easily distinguished from the myosin filaments, whereas in rigor the two filaments appear to have similar diameters. In the images of active fibers, the actin filaments appear to have diameters intermediate between those in rigor and in relaxed fibers. Closer inspection reveals characteristic differences also in the appearance and diameters of the myosin filaments in relaxed, rigor, and active fibers. For example, the thick filament perimeter frequently looks almost round in rigor, whereas it often looks irregular in the cross sections of active muscle.

In many cases thin lines of density ("crossbridges") can be seen between neighboring actin and myosin filaments. The sections are quite thin (~20 nm) and the crossbridges therefore are seen with much higher relative contrast than is usually seen in thicker sections. Crossbridges are prominent in the active and rigor images, but are clearly visible also in the relaxed fibers. The number of visible crossbridges extending from a single myosin filament to its six actin neighbors is variable, from none in some cases to the maximum of six in others (see Discussion). We have not observed any regular pattern in the distribution of these filled and empty potential crossbridge sites.

Fourier Transforms of Cross Sections

We used Fourier analysis to extract information about the average structure in the images. Each image was first corrected for geometric distortions of the filament lattice caused by the sectioning or other steps of the preparative procedure. A standard "unbending" procedure, as described in Materials and Methods, was used to recast each image onto a regular hexagonal lattice of constant spacing. Fourier transforms and power spectra were computed. Power spectra from a number of different images of each time point were summed to give a clearer picture of the intensity distribution. These summed power spectra are displayed as insets in each panel of Fig. 2. The highest resolution spots visible in the figure correspond to a spacing of 1/8.5 nm^{-1} ([4,0] and [3,2], visible most clearly at 300 ms), but in the numerical output of the summed power spectra there were significant peaks at the [1,5] lattice positions, corresponding to ~1/6 nm^{-1}. The highest resolution spots visible in power spectra from individual raw images before unbending were at a spacing of ~1/9 nm^{-1}.

Movements of mass from the vicinity of the thick filaments to the thin filaments is observed in x-ray experiments as a change in relative intensity of the [1,0] and [1,1] equatorial peaks in the fiber diffraction pattern (Huxley and Brown, 1967). For a number of reasons (see Discussion) only qualitative agreement between x-ray and our EM data can be expected. It is interesting nevertheless to compare changes upon activation in the [1,1]/[1,0] intensity ratio derived from our images with the corresponding x-ray measurements on live contracting muscle. Table I shows such a comparison.

Table I. [1,1]/[1,0] Intensity Ratios from EM and x-ray

	relax	rigor	20 ms	50 ms	80 ms	300 ms
EM[a]	0.5(0.2)	4.2(1.6)	2.8(1.3)	2.1(0.7)	1.7(0.4)	2.3(0.7)
x-ray[b]	1.3 *0.6*	4.3 *3.6*				1.6 *1.9*

[a] The ratio of the lattice reflections has been divided by $\sqrt{3}$ since the x-ray intensities are rotational averages: i.e., decrease in proportion to radius. The values are average (SD).
[b] From reference (Huxley, 1968), for rabbit psoas or, in italics, from (Haselgrove and Huxley, 1973) for frog sartorius. The 300 ms rabbit value is from (Brenner and Yu, 1985).

The values in the table are derived from intensities integrated over entire peaks, which are somewhat broadened as seen in the power spectra in Fig. 2. There is an approximate eightfold change in the [1,1]/[1,0] ratio comparing relaxed to rigor muscle. After ATP release, the ratio first decreases, then later increases again slightly. Our early time point measurements are not directly comparable to the available quantitative x-ray results, since our muscles are activated from rigor instead of from the relaxed state. At 300 ms, the muscle is generating maximal tension, so this time point should correspond roughly to the isometric contractions studied by x-ray diffraction (Haselgrove and Huxley, 1973; Brenner and Yu, 1985). As Table I shows, there is reasonable agreement between the pattern of changes in our data and that seen in x-ray experiments.

Fourier Filtration

The Fourier transforms of images at each time point were also used to calculate noise-filtered views of the average unit cells. In the A-band of rabbit muscle, the thick filament is surrounded by six thin filaments arranged on a hexagonal lattice. This arrangement gives sixfold rotational symmetry around the thick filament if we ignore the detailed structure of thick and thin filaments. If we consider the three-start helical structure of a thick filament, cross-sectional images of individual thick filaments should give threefold, not sixfold symmetry. However, the image of a myofibril as a whole does not have threefold symmetry, because the thick filaments in rabbit muscle are not rotationally aligned (Squire et al., 1990). We compared the phase residuals calculated on the assumption of either sixfold or threefold symmetry for our images of rigor muscle. The threefold residual was no smaller and often larger than the sixfold residual. Thus we calculated the averaged images assuming sixfold symmetry. All lattice reflections out to a resolution of 1/9 nm^{-1} were included in the Fourier syntheses. Fourier filtered data from several images (21 for rigor, 7 for relaxed, and 11 to 13 for activated fibers) were put into the same orientation and direction of view (see Materials and Methods) and then summed to make the final density maps. The average amplitudes and phases are listed in Table II. To make this data useful for Fourier filtration, we extracted the Fourier components located exactly on the reciprocal lattice positions only, not integrated over entire peaks. Thus the [1,1] and [1,0] amplitudes do not yield the same values for the [1,1]/[1,0] ratio as given for the integrated intensities in Table I. The results of the Fourier filtration are shown in Fig. 3 *a*. Only a portion

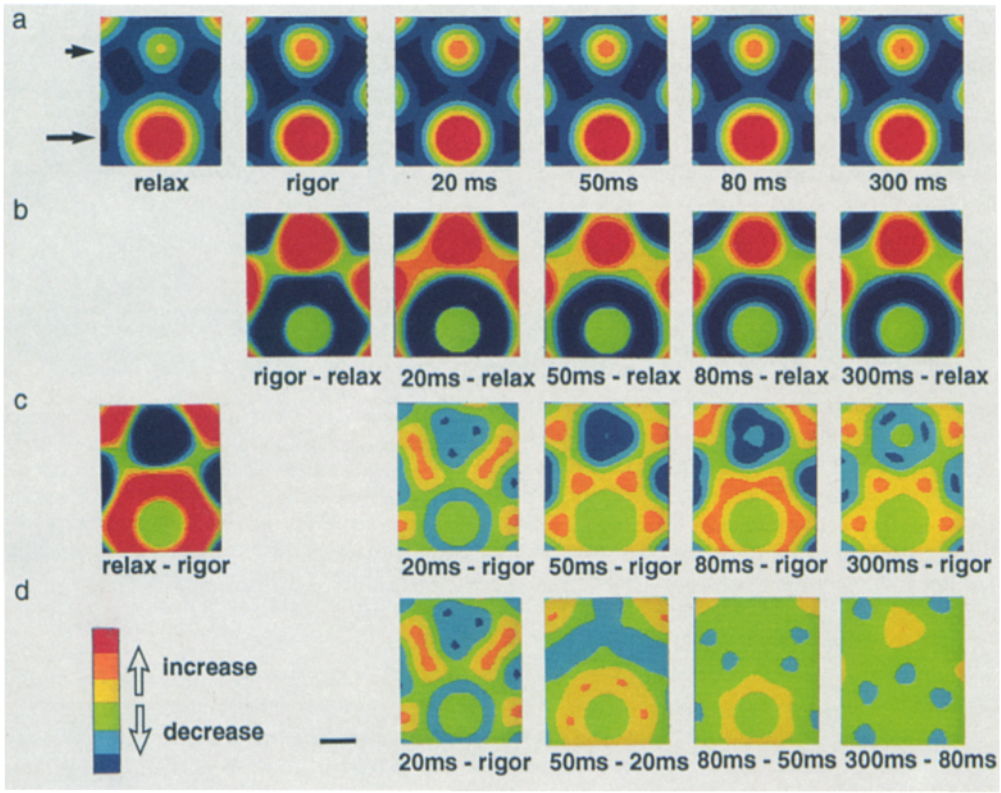

Figure 3. Fourier-filtered average images and difference maps derived from cross sections of fibers. In each case a portion of a unit cell containing one thick and one thin filament is shown. The complete image has sixfold rotational symmetry around the center of the thick filament. (*a*) The average appearance of cross sections of muscle fibers frozen while relaxed, in rigor, and at 20, 50, 80, and 300 ms after flash photolysis of caged ATP. The large and small arrows point to the myosin and actin, respectively. Red indicates higher density, blue lower, according to the pseudo-color intensity scale shown at the lower left of the figure. (*b*) Changes in intensity compared to relaxed muscle. The difference maps were computed as described in Materials and Methods. (*c*) Changes in intensity compared to muscle in rigor. (*d*) Sequential changes in intensity after release of ATP. Bar (located at the left end of the lower row), 10 nm.

of each unit cell is shown, since the calculated structure has sixfold symmetry around the center of the myosin filament.

The averaged density maps cannot show details of crossbridge shapes (since the crossbridges do not conform to p6 symmetry), but they do reveal the transfer of mass between thick and thin filaments, manifested as changes in apparent diameter and distribution of average mass around the filaments. The thick filament is noticeably larger in relaxed than in rigor, whereas the thin filament is smallest in relaxed, largest in rigor, and of intermediate size in the active muscle. By careful comparison, a number of other differences between the various time points can be seen, but a simpler way to visualize these changes is by calculating difference maps. Fig. 3 *b* shows the changes compared to relaxed muscle, Fig. 3 *c* the changes compared to rigor muscle.

Consider first the changes relative to relaxed muscle (Fig. 3 *b*). In rigor and at all times after the release of ATP, the difference maps show a strong positive density centered on the actin filament, and a strong annulus of negative density at the periphery of the myosin filament. The difference is largest in the map of *rigor-relax* and somewhat smaller in *50 ms-relax* or *80 ms-relax* (Fig. 3 *b*). Stated in terms of mass movement, the difference maps show a transfer of material from the myosin filament to the actin filament when a relaxed muscle goes into rigor or becomes active. This corresponds to the results described above in terms of the ratio of the [1,1] to [1,0] intensities in the power spectra. At 20 and to a lesser extent 50 ms, some of the transferred mass is located in the region between two actin filaments.

Relative to rigor (Fig. 3 *c*), the fiber at 20 ms after ATP release shows a significant decrease in density near the actin filament on the side facing the myosin filament. An increase in density is seen in the regions between the actin filaments. In other words, by 20 ms after release of ATP, mass has departed the actin filaments, but the net displacement has been azimuthal, rather than radial, so the mass has not yet returned to the thick filament. At 50 ms, the actin density has had a further significant decrease, and now the regions of positive density have moved radially to a position closer to the myosin filament. At 80 ms, the positive ring around the myosin filament is stronger and the positive regions between the actin filaments have disappeared. At 300 ms, the

Table II. Fourier Components (Normalized to IFI_{max} = 1000)

	[h,k]									
	[1,0]	[1,1]	[2,0]	[2,1]	[1,2]	[3,0]	[2,2]	[3,1]	[1,3]	[4,0]
	Phase									
	0	0	π	π	π	0	π	π	π	π
	IFI									
rigor	517	1000	63	89	50	16[a]	45	41	57	20
20 ms	492	1000	17[b]	41	43	72	13	41	44	28
50 ms	611	1000	25	47	44	79	16	35	45	9
80 ms	555	1000	65	86	70	68	11	51	57	31
300 ms	590	1000	25	74	59	75	13	35	36	18
relax	1000	910	66	59	50	58	1	15	18[c]	12

[a] 11 out of 21 of the rigor images had π for the phase of the [3,0] spot.
[b] 8 out of 11 of the 20 ms images had 0 for the phase of the [2,0] spot.
[c] 3 out of 7 of the relaxed images had 0 for the phase of the [1,3] spot.

actin region remains negative, and the myosin periphery remains positive compared to rigor, but the differences are substantially less than at earlier times.

The sequential changes on going from one time point to the next after ATP release are shown in Fig. 3 *d*. Comparing 50 to 20 ms (second map in Fig. 3 *d*) shows a movement of mass from the regions between the actin filaments towards the periphery of the myosin filament. A very slight continuation of this movement is the only net change between 50 and 80 ms. Between 80 and 300 ms, the direction of mass movement reverses, the net transfer now being from the periphery of the myosin filament to the actin filament.

Some of the images in Fig. 3 *c* reveal handedness. The density contours around the actin filament are not circular, but rather have the shape of a triangle with rounded edges. The apex of this triangle points slightly to the left of a line joining the centers of the actin and myosin filaments. This asymmetry shows up most clearly in the difference maps of Fig. 3 *c*, where the rigor image has been subtracted from the other time points, but on close inspection it is also visible in the rigor and 300 ms images of Fig. 3 *a*. In the Fourier transform, this right-left asymmetry is manifested as a difference between those pairs of spots that are mirror related but not sixfold related: the [2,1] and [1,2], or the [3,1] and [1,3] for example. As shown in Table II, the mirror asymmetry is most prominent in rigor, absent at 20 ms, then reappears somewhat in the 50, 80, and 300 ms transforms.

Correspondence Analysis of Crossbridge Images

Although the global averages obtained by Fourier synthesis are useful, a much more informative result can be obtained by taking account of the heterogeneity in the crossbridge population. Ideally we would like to average together only crossbridges of the same structural type. The problem of course is to recognize in the somewhat noisy images which crossbridges are the same type and which are different. We used correspondence analysis (van Heel, 1984; Bretaudiere and Frank, 1986; Greenacre, 1993; Lebart, 1993) to ferret out the major features that differentiate one crossbridge type from another. The crossbridges were obtained from the unbent images of cross sections by a semiautomated extraction (see Materials and Methods) of small rectangular regions such as shown in Fig. 4, each containing one actin filament and a neighboring myosin filament (an A-M pair). Approximately 10,000 A-M pairs per time point (70,957 total A-M pairs) were analyzed.

We masked out most of the backbone of the myosin filament, and the area outside the crossbridge region to exclude contributions near the edges that come from the neighboring actins and myosins. The eigenvectors of the pixel covariance matrix derived from these masked A-M pair images were identified by correspondence analysis. The 12 largest eigenvectors were used to classify the images of A-M pairs into 16 classes, as described in detail in Materials and Methods. For the various time points, 75–87% of the A-M pairs were classifiable into these 16 classes. Fig. 5 shows the characteristic appearance of each of these classes, both as reconstitutions of the centroid of each class (see Materials and Methods), and as interpretive sketches, drawn to emphasize the features used to distinguish between similar classes.

The important structural differences that distinguish the classes obtained from the correspondence analysis are as follows: (*a*) the presence or absence, and the strength of any density contours connecting the actin to the myosin (e.g., 7 vs. 8 vs. 14 vs. 16), as well as whether the connecting density has uniform width or is tapered (e.g., 6 vs. 1); (*b*) the apparent site of origin of the crossbridge on the myosin filament backbone—from directly underneath the actin (e.g., 2, 4, 7, 8, and 11), or rotated to the left (e.g., 1, 5, and 6) or right (e.g., 3, 9, 10, and 12) of the midline; (*c*) whether the crossbridge density profile appears straight (e.g., 7, and 8), or is bowed to the left (e.g., 1, 2, and 4) or to the right (e.g., 11 and 12); (*d*) the apparent diameter of the actin filament (e.g., 1 vs. 6).

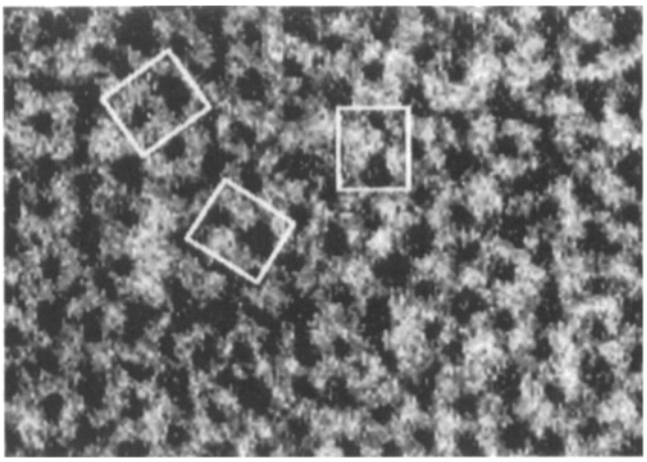

Figure 4. Extraction of individual A-M pairs for correspondence analysis. Rectangular areas such as shown by the white boxes in the figure (27 by 23 pixels, measuring ~42 × 36 nm), were cut out of unbent images of thin cross sections as described in Materials and Methods. Each box included one myosin and one actin. Every adjacent actin–myosin pair was extracted from each of the cross sections analyzed, ~10,000 pairs for each time point.

The first 12 of the classes have a strong continuous density connecting the actin to the myosin, and this density has a characteristic shape in each class. We interpret these densities as different shapes or orientations of crossbridges. Similar shapes of the myosin head may appear as two different density profiles because their sites of origin on the myosin filament differ, and they are thus forced to approach the actin filament from different angles. A likely example of this sort of difference is seen by comparing classes 1, 2, and 3. In all three cases, there is extra mass on the bottom-left side of the actin profile, indicating that the head region of a crossbridge (the motor domain) is located there. The crossbridge density tapers near the thick filament. In class 1, the apparent site of origin of the crossbridge is located to the left of the midline, whereas in class 2 it is on the midline, and in class 3 it is located to the right. In these three classes the left side of the outline of the crossbridge density is curved outward in the region near the thin filament, but the right side is almost straight. This gives the impression that crossbridges approach the thin filament from the left side. Crossbridges in classes 4–6 have different shapes from classes 1–3, but they also all seem to approach the actin filament from the left. Here we call the crossbridges in classes 1–6 left-handed crossbridges. Crossbridges in classes 9, 10, 11, and 12 are, approximately, the mirror images of 6, 5, 4, and 1, respec-

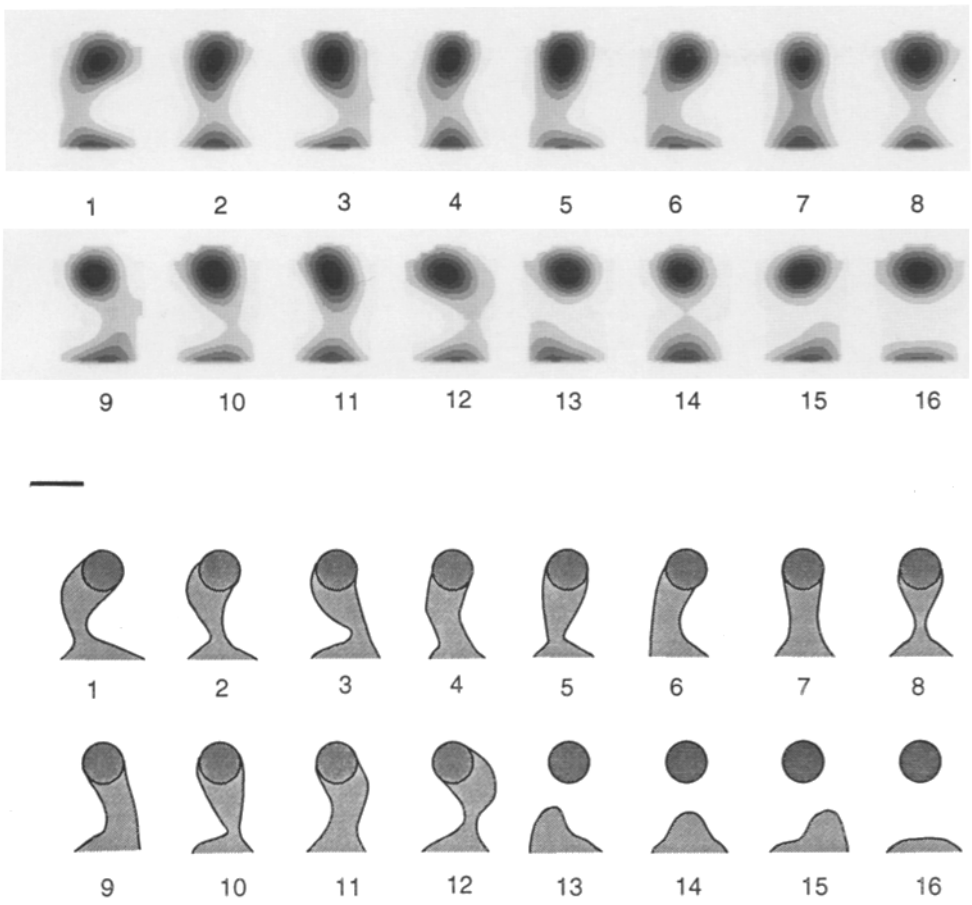

Figure 5. Images (*top two rows*) and interpretive sketches (*bottom two rows*) of the 16 structural classes identified by correspondence analysis. Each image extends from a single actin filament near the top to the periphery of the thick filament backbone at the bottom. Bar (between second and third row), 10 nm.

tively; they seem to approach the thin filament from the right side (right-handed crossbridges). Crossbridges in classes 7 and 8 are straighter and approach the thin filament from directly below (straight crossbridges).

The images that fall into classes 13 to 15 each have a lobe of density protruding from the thick filament, probably corresponding to detached heads. Although it was sometimes difficult to decide whether these densities are connected to the thin filament or not, images in these classes generally had a thin filament with a smooth round contour, surrounded by lower density. Images in class 16 have very low density between the thick and thin filaments, probably corresponding to A-M pairs without myosin heads in this direction (see Discussion).

Table III shows the proportion of A-M pairs falling into each class at different time points. The rigor and relaxed fibers have a relatively narrow distribution. Classes 1, 2, and 3 are high in rigor and less than 0.5% of the total in relaxed. In contrast, classes 13, 14, and 15 are high in relaxed and less than 0.5% in rigor. The activated fibers show wider distributions, but still there are clear differences. For example, class 8 has a maximum at 50 ms, then decreases at later times, whereas class 10 is highest at 300 ms. Rigor fibers had a preponderance of left-handed crossbridges over right-handed (56% in classes 1–6 vs. 5% in 9–12). This preponderance diminishes soon after activation and recovers at later times. This is consistent with the handedness revealed by the Fourier averaged density maps (Fig. 3). Straight cross-

Table III. Classes of Crossbridges Identified by Correspondence Analysis

	No. of A-M pairs	Classifiable A-M pairs	Distribution of A-M pairs among classes %															
			1	2	3	4	5	6	7	8	9	10	11	12	13	14	15	16
Relaxed	19066	17985	0	0	0	0	0	9	7	2	7	2	0	0	15	10	12	36
Rigor	7508	6554	16	29	9	0	2	0	0	8	0	0	2	3	0	0	0	31
20 ms	10797	9632	5	12	4	0	2	8	4	9	3	7	4	4	2	0	4	32
50 ms	10055	8347	0	2	0	4	2	15	5	18	11	5	2	2	2	2	0	30
80 ms	12289	10191	4	5	2	4	2	8	5	12	4	10	5	5	2	0	4	28
300 ms	11242	9407	8	5	6	4	7	9	3	9	3	13	5	2	0	0	2	24

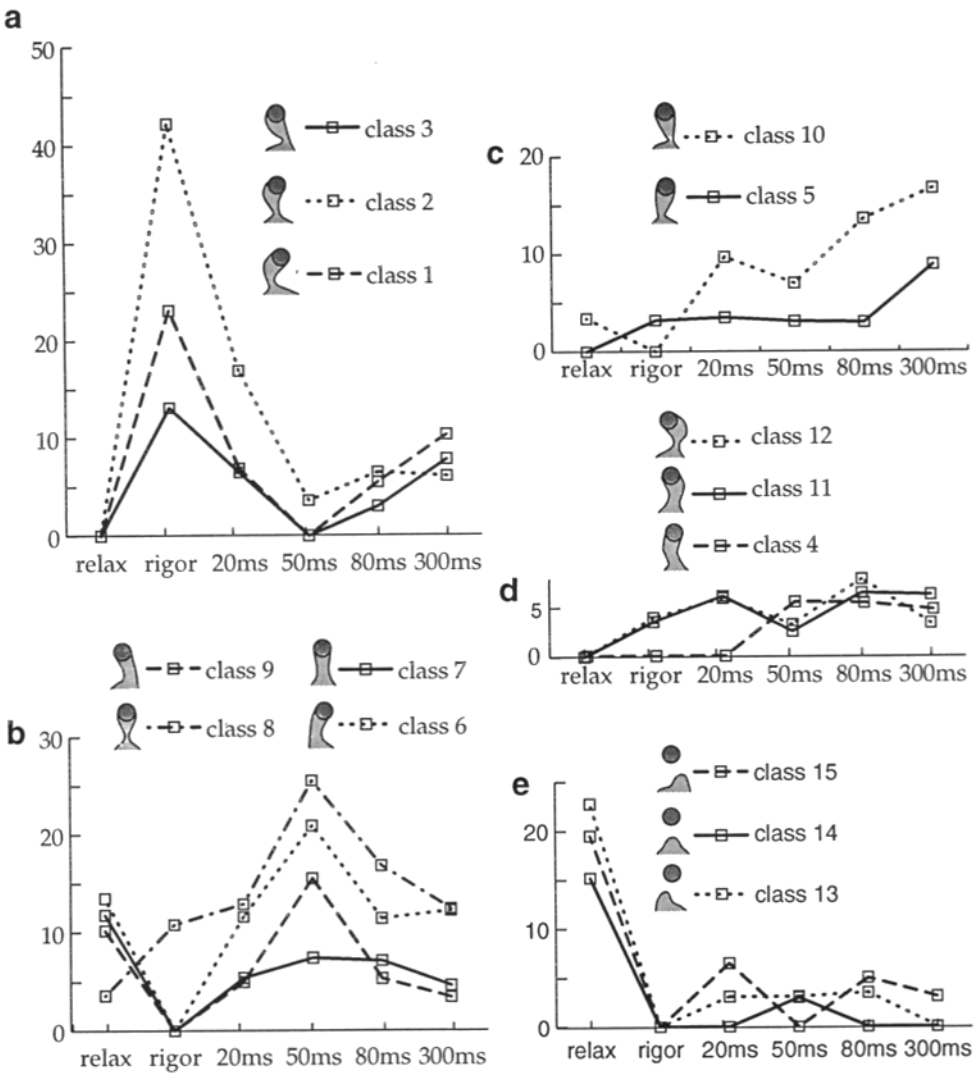

Figure 6. Time course of changes in the structure of crossbridges. The proportion of each of the classes identified by correspondence analysis is shown for muscles that are relaxed, in rigor, or at 20, 50, 80, and 300 ms after release of ATP. Classes that exhibit a similar time course have been plotted together in the same graph. Numbers on the vertical axes indicate percentages of the sum of classes 1–15.

bridges (classes 7 and 8) were few in rigor, but fairly frequent in contracting muscles, especially at 50 ms.

Time Course of Structural Changes in the Crossbridge

To simplify further interpretation of this distribution of crossbridge shapes, we will exclude class 16, the A-M pairs which simply lack available myosin heads. This class accounts for ~30% of the total images at all time points, a value that is determined primarily by section thickness (see Discussion). For all subsequent analysis, class 16 has been removed and the proportions have been recalculated on the basis of the total of classes 1 to 15 only.

A helpful way of visualizing the distribution is to view the changes in each class as a function of time. When this is done, each class is found to have a distinctive time course, but they all fit roughly into five time profiles, plotted in Fig. 6, *a–e*. The first pattern, shown by classes 1, 2, and 3 (Fig. 6 *a*) has a very low value in relaxed fibers and is very high in rigor, drops to less than half at 20 ms, has a minimum at 50 ms, then slightly increases at 80 and 300 ms. The second pattern, Fig. 6 *b* (classes 6, 7, 8, and 9) shows some variability, but essentially these classes peak at 50 ms (especially 6, 8, and 9). Classes 6, 7, and 9 are very low in rigor, and higher in relaxed fibers. Most of the attached crossbridges in relaxed fibers belong to these three classes. Classes 5 and 10 (Fig. 6 *c*) make a third pattern with a maximum at 300 ms. The fourth pattern, formed by classes 4, 11, and 12 (Fig. 6 *d*) consists of relatively minor populations that exist mainly in active fibers. Finally, a fifth pattern is characteristic of classes 13, 14, and 15 (Fig. 6 *e*), which exist mainly in relaxed fibers, are not seen in rigor, and constitute a very small fraction of the crossbridges in active fibers at all time points.

The similarities among the time courses observed for different classes suggests a consolidation of the classes into functional groups. We can label these time profiles with terms that are useful for connecting our structural data to the known biochemical and mechanical events of muscle activation. Fig. 6 *a* is thus denoted a rigor pattern; Fig. 6 *e* is a relaxed pattern, Fig. 6 *b* is an early active phase, and Fig. 6 *c* is a mature contraction phase. Table IV presents the data regrouped in this fashion. Although this grouping is based on the time course of the populations, there are some structural similarities among the class images within a group. For example, classes 1, 2, and 3 share common structural features as described above. They have a large actin profile and the density tapers near the thick filament. The crossbridge density of class 5 and 10 also tapers near the thick filament,

Table IV. Crossbridge Classes Grouped by Time Course

	3 1 2	5 10	8 9 6 7	12 4 11	15 13 14
Relaxed	0	3	39	0	58
Rigor	78	3	11	8	0
20 ms	30	13	35	12	10
50 ms	4	10	69	11	6
80 ms	15	17	41	19	8
300 ms	24	26	33	14	3

but the center lines of the density in these images are not bowed as in class 1 or 2. The images in classes 6, 7, and 9 are similar in that the actin filament has a small profile and the crossbridge density has almost uniform width. The crossbridges in class 4 and 11 also have uniform width, but are slightly bent. The densities in classes 13–15 are not connected to the thin filament and are thus thought to be detached myosin heads. Considering these structural similarities, the different shapes within each time course grouping appear to be crossbridges that have a similar conformation for the motor domain but originate from different azimuthal positions on the myosin filament. Thus grouping the classes solely on the basis of the time course of their population changes has yielded groups that would reasonably be assembled based on structural considerations.

One or more of the crossbridge shapes that are dominant in the rigor images should contain a motor domain that matches that part of the structure of S-1 in the recently published crystal structure and in the 3-D reconstruction of decorated actin filaments. Fig. 7 shows a comparison of the strongly curved rigor crossbridge (class 1) with data from the 3-D reconstruction of acto–S-1 by Milligan and coworkers (Milligan and Flicker, 1987). The acto–S-1 contours represent an axial projection of an actin filament containing two adjacent attached S-1's, corresponding to a two-headed crossbridge. As seen in the figure, the two structures match quite well near the actin, but deviate somewhat nearer the thick filament backbone.

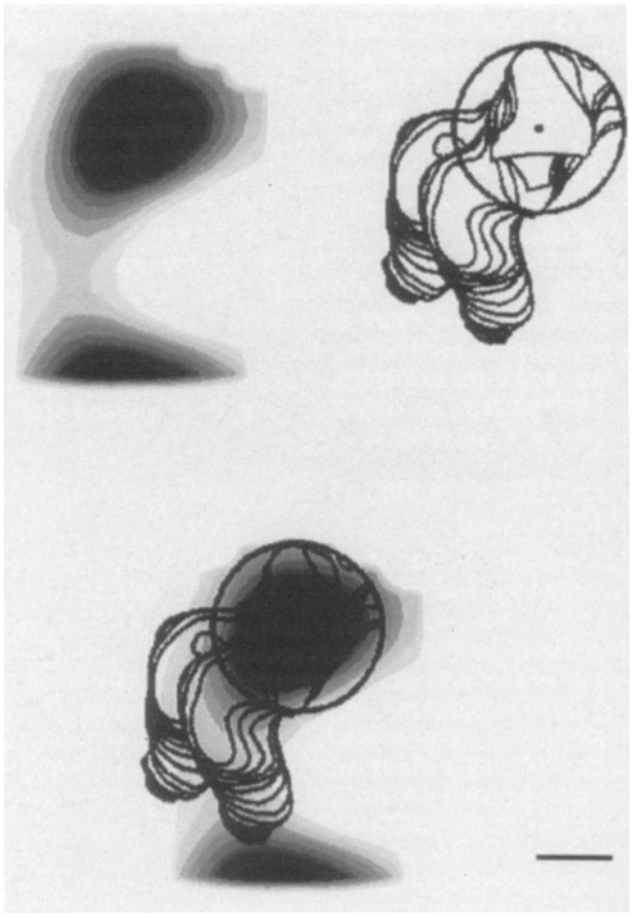

Figure 7. Comparison of a rigor crossbridge with the electron density map of acto–S-1. Contours from the map of acto–S-1 (Milligan and Flicker, 1987) viewed down the actin filament axis are shown as black lines. The contours represent the outlines of two S-1 molecules bound to adjacent actins along one strand of the actin helix, plus a circle to indicate the approximate outer border of an extended length of actin filament. The density distribution within our class 1 is shown as a gray scale image. At the bottom of the figure, the two are superimposed. Bar, 5 nm.

Discussion

The most important conclusion from our data is that we have directly observed structural changes in the crossbridge that precede and accompany generation of force. This structural change has been a postulate for most models of muscle contraction. There has been strong indirect evidence from x-ray and probe studies of muscle and EM observation of acto–myosin complexes in vitro that such changes do occur. However, direct observation of changes in crossbridge structure correlated with onset of force production in muscle has until now been lacking. In this paper we have identified several attached crossbridge shapes that differ from rigor crossbridges and were more prominent during force development than at steady-state. Shifts among these populations are temporally correlated with force development. We need to consider several issues to put together a satisfactory interpretation of these structural changes in terms of what we already know about the biochemistry, mechanics, and structural correlates of muscle contraction. Although we will discuss our results in terms of their implications for the mechanism of force generation, it is important to bear in mind that the transition we actually observe is not between relaxation and full activity, but between rigor and full activity. This transition may correspond to the sequence of events between the nucleotide free state and the force generating states of the subsequent cycle.

Trapping of Transient States by "Flash and Smash"

In rabbit psoas fibers at 20°C, ~300 ms are required to complete each cycle of the actomyosin ATPase reaction (Goldman, 1987). Force develops over a period of ~100 ms after ATP release. Our rapid freezing apparatus stops motion of proteins within ~1 ms (Heuser et al., 1979) by impact with a liquid helium-cooled copper block. The minimum time interval between the laser pulse ("flash"), which photolyzes caged ATP, and contact with the freezing block ("smash"), is ~15 ms. At any time from 15 ms after ATP release to completion of the first biochemical cycle, the time required to trap the current crossbridge population (1 ms) is very short

compared to the time course of force development. Preservation of native ultrastructure is known to be excellent with freeze-substitution (Bridgman and Reese, 1984; Craig et al., 1992; Sosa et al., 1994). Sections of an intrinsically well-ordered protein sample give lattice reflections smaller than 3 nm (Hirose et al., 1993). Vertebrate muscle is less well-ordered, but freeze-substitution of muscle followed by Fourier analysis of micrographs of thin sections gives lattice reflections of 6–7 nm (Lepault et al., 1991; Hirose et al., 1993; Lenart et al., 1993; Sosa, H., E. Ouyang, and H. E. Huxley. 1993. *Biophys J.* 64:26a; Sosa et al., 1994). The highest resolution lattice spots seen in power spectra from our images of cross sections are $\sim$1/6 nm^{-1}. The statistically significant differences identified by correspondence analysis between the different classes of crossbridge shapes extend to a resolution of $\sim$3 nm.

Limitations of Viewing 3-D Structural Changes in 2-D Projection

Our images are 2-D projections of the crossbridges contained in thin cross sections. If there are two different conformations of the crossbridge that differ from each other in the direction of the filament axes, but are identical in mass distribution in the radial and azimuthal directions, then they will be lumped together in a single class by our procedures. It is likely that an active crossbridge would bear quite different loads, depending on the distance from its site of origin on the thick filament to the particular actin it happened to bind. Since the repeat lengths of the thick and thin filaments are mismatched, there will be crossbridges that have the same configuration of the myosin head and the same azimuthal angle but generate different amounts of force due to different axial displacements between their site of origin and their actin binding site. Viewing the specimen in 2-D axial projection, such crossbridges would be placed in the same structural class even though they are mechanically quite different.

Since our sections are slightly thicker than the subunit periodicity of the myosin filaments, some of the images must contain two superimposed crossbridges. It is reasonable to ask how much of the variation in crossbridge shape that we see could be accounted for by artifacts of this superposition. The present results identified prominent classes of attached, non-rigor–like, crossbridges. If, for example, some crossbridge images observed in active fibers are the superposition of rigor-like crossbridges and detached crossbridges, the resultant images may appear to contain a third class of shapes. Even without superposition, an apparent third class might be generated from only two states of the myosin if the two heads of a single myosin molecule were in different states. The effects of these possible artifactual sources of apparent structural change on the distribution of observed shapes were investigated by extensive model calculations. Due to space limitations, these calculations must be published separately (K. Hirose, manuscript in preparation), but they are summarized briefly below.

About 70% of the A-M pair images from each time point showed clear density profiles between the thin and thick filaments corresponding to myosin heads, whereas 30% did not have such density. In thin sections a certain proportion of A-M pairs should lack crossbridges, since one crown of a thick filament has only three myosin molecules to make crossbridges to six neighboring thin filaments. In thicker sections the percentage of these empty A-M pairs should decrease. From the proportion of empty A-M pairs, we calculated an apparent section thickness of 23.2 nm, in good agreement with the microtome setting (20 nm). The apparent section thickness was the same in relaxed, rigor, and active fibers. From the section thickness we can directly calculate the proportion of A-M pair images that should contain two superimposed crossbridges. The estimated percentage of these overlapped crossbridges was less than 15%.

We attempted to simulate our observed distribution of crossbridges among multiple structural classes using only two or three basic shapes superimposed on one another, but found that the small and constant fraction of superimposed crossbridges (15%) rules out such an explanation. We also could not account for the observed distributions by a mixture of single and double-headed crossbridges containing heads in a small number of different states. Thus, we think that most of our different classes do represent distinct structural conformations of individual crossbridges. The number of distinct biochemical states of the motor domain is probably smaller than the number of structural classes, as discussed below.

Since the origin of the crossbridge on the myosin filament can have nine different azimuthal orientations, there are at least three different positions for the crossbridge origin relative to each thin filament. Moreover, actin molecules in the thin filament helix have several different azimuthal orientations, which would also change the shape of crossbridges. Axial displacement due to the mismatch of the thin and thick filaments could also change the crossbridge appearance in the cross sections. Thus, it is reasonable to expect several different crossbridge shapes even for a single biochemical state of the motor domain. These shape differences are probably particularly noticeable in the stem and neck region of the crossbridge. A very clear illustration of this effect was previously seen as part of the difference between lead and rear crossbridges in rigor insect flight muscle (Reedy and Reedy, 1985; Taylor et al., 1986, 1989).

Correlation of Structural, Biochemical, and Mechanical States

The density between thick and thin filaments was continuous in some of the classes (1–12), and discontinuous in others (13, 14, and 15), probably corresponding to attached and detached crossbridges. The attached crossbridges had more than one shape even in rigor fibers that are expected to be in a uniform biochemical state. Since we distinguished three major different shapes for crossbridges in rigor fibers that probably have a single conformation of the motor domain, we might expect that other biochemical states of the crossbridge would also be represented by about three structural classes. Our 15 different classes then probably represent approximately five different motor domain conformations. In fact, the 15 classes fall naturally into five groups based on the time course of changes in their distribution.

Detached crossbridges (classes 13, 14, and 15), presumably myosin-ATP or myosin-ADP-Pi, were most prominent in relaxed fibers and virtually absent in rigor as expected. The detached crossbridges increased at early times after activation from rigor and decreased slightly at later times. This result is consistent with the changes in the [1,1]/[1,0] ratio. However, we cannot use this result to estimate the correct

proportion of attached heads, because the remaining attached crossbridge images could contain myosin molecules with one head attached and the other detached, and also could contain heads that are located near the thin filament but not actually bound. EM and EPR studies suggested that crossbridges in the presence of nucleotide are single-headed (Fajer et al., 1988; Stein et al., 1990; Frado and Craig, 1992; Berger and Thomas, 1993).

In relaxed muscle three classes of attached crossbridges are present (6, 7, and 9). Since the stiffness of relaxed muscle is very low under our conditions (Brenner et al., 1982), these probably correspond to weakly attached forms. They are similar to each other in their time courses and probably are the differing structural manifestations of a single attached conformation of the motor domain. This triplet is absent in rigor, and increases rapidly after ATP release. The population has its peak at 50 ms (~40%), where we expect a substantial fraction of crossbridges to be in an initial attachment step, and decreases to ~20% at 300 ms. All three of these classes had crossbridge density with a relatively uniform width between thick and thin filaments. This is similar to some of the individual crossbridge images observed during steady contraction in previous work (Hirose and Wakabayashi, 1993) and also consistent with the changes seen upon addition of AMPPNP to insect muscle fibers in rigor (Reedy et al., 1988).

The shift from rigor crossbridges (classes 1, 2, and 3) to these uniform crossbridges (classes 6, 7, and 9) is probably responsible for the increase of mass near the thick filaments after activation observed in the Fourier averaged images. We checked the possibility that this sort of uniform crossbridge could be composed of one rigor-like head and one detached head, since that combination might cause a crossbridge image with uniform width. Our model calculations (K. Hirose, manuscript in preparation) showed that the observed time courses can not be explained by such a combination of rigor and detached heads. At least one of the myosin heads in these classes must be attached by a conformation that is different from rigor. The general conclusion that we can draw from these model calculations is that three or more *attached* conformations of the motor domain of the crossbridge are needed to satisfactorily account for the present observations.

Structural Changes and Force Production

If we accept the interpretation that classes 6, 7, and 9 are weakly attached, then some or all of the remaining attached non-rigor crossbridge forms must be responsible for actively generating force. For example, 5 and 10 are a set of classes that share similar shapes and time courses. Classes 4 and 11 comprise another such group. The total percentage of these four classes is low in relaxed or rigor fibers, ~20% at 20 to 50 ms, 30% at 80 ms, and 40% at 300 ms, which is roughly in parallel with tension development. Thus, at least some of these shapes (5, 10, 4, and 11) are likely to be a conformation of strongly attached, force-producing crossbridges.

The percentage of these four classes is not, however, exactly proportional to the force. Likewise, no other subset of the 15 classes has a combined population that is a quantitative predictor of tension. Tension would not be proportional to a simple sum of the populations if more than one structural class can generate force, and the amount of force per crossbridge is not the same for different classes. This differential force could be a real physiological characteristic of different structural classes, but it might also arise artifactually if we are unable to distinguish some of the crossbridges that belong to different mechanical states but have similar shapes in 2-D projection. In this study we used the cross-sectional view because the alignment of the A-M pair images is relatively simple and unique. However, to produce net force for filament sliding, we expect some axial movement of crossbridges, which cannot be directly observed in the cross-sectional view. Of course it is difficult to imagine that crossbridges can change their appearance only in the cross-sectional view without also changing shape when viewed laterally: the shape changes we have observed in cross sections are probably closely related to the conformational change of the three-dimensional crossbridges as a whole, which might be detected by correspondence analysis of longitudinal sections or 3-D reconstructions.

Comparison of Our Results with X-ray Diffraction Studies

X-ray experiments often measure the ratio of the [1,1] and [1,0] equatorial reflections as an indicator of mass associated with the thick and thin filaments. Qualitative agreement has previously been found between x-ray and EM measurements of the shift of material from thick to thin filaments when the muscle is switched from the relaxed to the rigor state (Huxley, 1968). Precise numerical agreement is not expected for the following reasons: (*a*) the x-ray data comes from a fiber or, more commonly, many fibers. Each fiber contains a mosaic of myofibrils with random azimuthal orientations. The resultant x-ray scattering is an average of the scattering from all azimuthal orientations of the filament lattice. In contrast, our EM images are from sections less than one unit cell thick of a single myofibril. (*b*) The x-ray data is also an average over both halves of the sarcomere. These two forms of averaging destroy the difference between the reflections that are mirror related but not sixfold related ([1,2] vs. [2,1]; [1,3] vs. [3,1], etc.). (*c*) The x-ray data averages over the entire sarcomere—I band, A band and H zone—where the relative amounts of actin and myosin differ greatly. The x-ray equatorial intensities therefore change with sarcomere length, so our cross sections give lattice reflections corresponding most closely to the x-ray data at full overlap. (*d*) Finally, the contrast we observe in our images arises mostly from electron scattering from the nuclei of heavy metal ions adsorbed to the muscle proteins, a process that is only approximately proportional to the protein electron density giving rise to contrast in the x-ray diffraction experiments. These factors that limit direct comparison are not, however, expected to change much with activation of the muscle, so the changes in our lattice reflections should parallel changes in x-ray scattering, as indeed they do.

A graph of the time course of change in the [1,1]/[1,0] x-ray intensity ratio following release of ATP in rabbit psoas by flash photolysis has also been reported (Poole et al., 1991). In that study the initial drop in the [1,1]/[1,0] ratio occurred very quickly (half time <5 ms), but it is not clear from the data shown whether there was any change in ratio between 50 and 300 ms after ATP release. The overall change from rigor to active muscle was said to be rather small, but no numerical values were given (Poole et al., 1991). In other published steady-state x-ray measurements, on rabbit psoas

(Brenner and Yu, 1985), rat soleus (Honda et al., 1993), and frog sartorius (Haselgrove and Huxley, 1973), the [1,1]/[1,0] intensity ratio decreases approximately twofold between rigor and active muscle, as in our data.

When we consider activation from the rigor state, the first change that occurs is movement of crossbridge mass away from the actin. Our Fourier averaged images show that the net effect is initially an azimuthal displacement into the region between the thick and two of its neighboring thin filaments. Later, between 20 and 50 ms, the movement has more of a radial component and the density near the surface of the thick filament increases. This suggests that, although the [1,1]/[1,0] ratio at 20 ms is intermediate between the values in rigor and at 50 ms, the crossbridge shapes at 20 ms are not simply a mixture of rigor and 50 ms shapes. There must be either detached crossbridges that have moved azimuthally and have not come back to the myosin filament region, or attached crossbridges that have a different shape than in rigor. Alternatively, one head of each crossbridge could be still attached as in rigor, affecting the conformation of the second head. There is little net change between 50 and 80 ms, but from 80 to 300 ms the net movement is back towards the thin filament, suggesting some additional conformational change from the initial attachment step to the force producing state.

The phases of the lattice reflections are not available directly from x-ray measurements, but several groups have assigned plausible phases on the basis of model calculations. For the first five reflections seen by x-ray ([1,0], [1,1], [2,0], [2,1], [3,0]), most authors (Haselgrove et al., 1976; Yu et al., 1985; Irving and Millman, 1989; Yu and Brenner, 1989; Harford and Squire, 1992) have chosen the values 0, 0, π, π, 0, in agreement with our measurements (Table IV). Yu and Brenner (Yu et al., 1985; Yu and Brenner, 1989) thought 0, 0, π, 0, 0, might be a better choice for relaxed rabbit muscle.

The phases of all reflections out to the [1,3] have also been directly determined from the Fourier transform of images of cryo-sections of rabbit psoas muscle, relaxed and in rigor (Trus et al., 1989). Their phases for the first five reflections were 0, 0, (π), π, (π) for relaxed, and 0, 0, π, π, (0) for rigor fibers (parentheses indicate uncertain phases). Our corresponding phases are 0, 0, π, π, 0 for relaxed and active muscles and 0, 0, π, π, (0) for rigor. Thus our phases agree well with the phases from frozen sections. Their amplitudes for both rigor and relaxed muscles agree quite well with our data in rigor. The relaxed cryo-sectioned muscle was, however, prepared in lower ionic strength than ours and very much more similar to rigor muscle than expected from x-ray measurements or from our EM data.

Comparison of Our Results with Previous EM and Spectroscopic Studies

Much previous work with spectroscopic probes (Fajer et al., 1990; Tanner et al., 1992; Allen et al., 1993; Ostap et al., 1993), EM studies on muscle proteins in vitro (Applegate and Flicker, 1987; Frado and Craig, 1992; Funatsu et al., 1993; Walker et al., 1994) or in muscle fibers during steady contraction (Hirose and Wakabayashi, 1993), and our own earlier EM study of longitudinal sections of flash activated muscle fibers (Hirose et al., 1993), have suggested that the homogenous population of crossbridges present in rigor is rapidly replaced by a less well-ordered population when ATP becomes available. In the present study we find that 90% of the crossbridges in rigor are accounted for by just four different shapes, and three of these account for 80% of the total. By 20 ms, 10 different shapes are needed to represent 90% of the crossbridges. This rapid diversification agrees with the early onset of disorder seen following ATP release in most previous work, but one study reported an ordered arrangement of S-1 binding to actin that changed little in the presence of ATP (Pollard et al., 1993).

We recognized three shapes of crossbridges in rigor (1–3) which are most likely attached by the same "rigor conformation" of the motor domain, but differ by the location of the origin of the crossbridge on the thick filament and the azimuthal orientation of the bound actin molecule within the thin filament helix. All of the major classes present in rigor (1, 2, 3, and 8) had crossbridge density that is wide and strong near the thin filament and narrower near the thick filament. This concentration of mass near the thin filament is consistent with the previous observations in both longitudinal and cross sections of rabbit (Hirose et al., 1993; Hirose and Wakabayashi, 1993) and insect (Taylor et al., 1984, 1986) muscle, and in deep-etch images of fish, crayfish, and insect muscle (Heuser, 1983; Varriano-Marston et al., 1984; Bard et al., 1987), which showed triangular shapes with their base at the actin filament for the rigor crossbridges.

After activation the percentage of the rigor-like crossbridges (1, 2, and 3) decreased from 80% to almost none, but recovered to ~20% at later times. Measurements of ATP release and utilization under conditions similar to ours (Ferenczi et al., 1984) rule out ATP depletion as a cause for reappearance of these rigor-like bridges. This is consistent with EPR results suggesting that 20% of the heads during steady contraction are highly ordered and oriented as in rigor (Fajer et al., 1990).

The shape of the S-1 portion of the myosin head in its rigor conformation has been determined both by EM (Milligan and Flicker, 1987; Rayment et al., 1993*a*) and by x-ray diffraction from crystals (Rayment et al., 1993*b*). Fig. 7 is a comparison of the known profile in 2-D projection of rigor S-1 (Milligan and Flicker, 1987) with our data from rigor muscle. We expect our data to match the in vitro structure over the region near the actin filament, but differ somewhat more distally. In our muscle fibers, the two heads must be joined together into a common stem leading to the thick filament, whereas the terminal portions of the S-1 in vitro are not constrained. For the S-1 portion of the crossbridge near the actin filament, there is good agreement between our data and the published structures. We conclude that our classes give a reasonably accurate picture of the structure of the crossbridge viewed in 2-D axial projection.

Conclusion

We have observed in 2-D axial projection the structure of the crossbridges in relaxed muscle, in rigor, and after activation from rigor by flash photolysis of caged ATP. The distribution of crossbridge shapes changes dramatically between relaxed, rigor, and with time after ATP release. In relaxed muscle, most crossbridges are detached. In rigor, all are attached with a small set of characteristic shapes that matches the known structure of the myosin head region when attached to actin from different sites of origin on the thick filament. Im-

mediately after ATP release, before significant force has developed (20 ms) the homogeneous rigor population is replaced by a much more diverse collection of crossbridge shapes. Over the next few hundred milliseconds, the proportion of attached crossbridges changes little, but the distribution of the crossbridges among different structural classes continues to evolve. Some forms of attached crossbridge (presumably weakly attached) increase at early times when tension is low. The proportion of other attached non-rigor crossbridge shapes increases in parallel with the development of active tension. The results lend strong support to models of muscle contraction that have attributed force generation to structural changes in attached crossbridges.

We thank Ms. X. Sun and Ms. N. Glaser for expert technical assistance, and Dr. Richard Tregear for helpful comments on the manuscript.

Supported by National Institutes of Health grant HL15835-21-25 to the Pennsylvania Muscle Institute, National Science Foundation grant MCB91-13313 to J. M. Murray and by fellowships from the Naito Foundation, the Muscular Dystrophy Association, and the Ciba-Geigy Foundation to K. Hirose.

Received for publication 11 May 1994 and in revised form 27 July 1994.

References

Allen, T. S., N. Ling, Y. E. Goldman, and M. Irving. 1993. Kinetics of orientation changes of rhodamine probes on myosin regulatory light-chains in skinned muscle-fibers following photolysis of caged ATP. *Biophys. J.* 64:231.

Applegate, D., and P. Flicker. 1987. New states of actomyosin. *J. Biol. Chem.* 262:6856-6863.

Bard, F., C. Franzini-Armstrong, and W. Ip. 1987. Rigor crossbridges are double-headed in fast muscle from crayfish. *J. Cell Biol.* 105:2225-2234.

Berger, C. L., and D. D. Thomas. 1993. Rotational dynamics of actin-bound myosin heads in active myofibrils. *Biochemistry.* 32:3812-3821.

Brenner, B., and L. C. Yu. 1985. Equatorial x-ray diffraction from single skinned rabbit psoas fibers at various degrees of activation. Changes in intensities and lattice spacing. *Biophys. J.* 48:829-834.

Brenner, B., M. Schoenberg, J. M. Chalovich, L. E. Greene, and E. Eisenberg. 1982. Evidence for cross-bridge attachment in relaxed muscle at low ionic strength. *Proc. Natl. Acad. Sci. USA.* 79:7288-7291.

Bretaudiere, J. P., and J. Frank. 1986. Reconstitution of molecule images analysed by correspondence analysis: a tool for structural interpretation. *J. Microsc. (Oxf.).* 144:1-14.

Bretaudiere, J. P., G. Dumont, R. Rej, and M. Bailly. 1981. Suitability of control materials. General principles and methods of investigation. *Clin. Chem.* 27:798-805.

Bridgman, P. C., and T. S. Reese. 1984. The structure of cytoplasm in directly frozen cultured cells. I. Filamentous meshworks and the cytoplasmic ground substance. *J. Cell Biol.* 99:1655-1668.

Calinski, R. B., and J. Harabasz. 1974. A dendrite method for cluster analysis. *Comm. Statistics.* 3:1-27.

Craig, R., L. Alamo, and R. Padron. 1992. Structure of the myosin filaments of relaxed and rigor vertebrate striated muscle studied by rapid freezing electron microscopy. *J. Mol. Biol.* 228:474-487.

Craig, R., L. E. Greene, and E. Eisenberg. 1985. Structure of the actin-myosin complex in the presence of ATP. *Proc. Natl. Acad. Sci. USA.* 82:3247-3251.

Diday, E. 1971. La methode des nuees dynamiques. *Rev. Stat. Appl,* 19:19-34.

Dubes, R. C. 1987. How many clusters are best? - An experiment. *Pattern Recogn.* 20:645-663.

Fajer, P. G., E. A. Fajer, N. J. Brunsvold, and D. D. Thomas. 1988. Effects of AMPPNP on the orientation and rotational dynamics of spin-labeled muscle cross-bridges. *Biophys. J.* 53:513-524.

Fajer, P. G., E. A. Fajer, and D. D. Thomas. 1990. Myosin heads have a broad orientational distribution during isometric muscle contraction: time-resolved EPR studies using caged ATP. *Proc. Natl. Acad. Sci. USA.* 87:5538-5542.

Ferenczi, M. A., E. Homsher, and D. R. Trentham. 1984. The kinetics of magnesium adenosine triphosphate cleavage in skinned muscle fibres of the rabbit. *J. Physiol. (Lond).* 352:575-599.

Flicker, P. F., R. A. Milligan, and D. Applegate. 1991. Cryo-electron microscopy of S1-decorated actin filaments. *Adv. Biophys.* 27:185-196.

Frado, L. L., and R. Craig. 1992. Electron microscopy of the actin-myosin head complex in the presence of ATP. *J. Mol. Biol.* 223:391-397.

Frank, J. 1990. Classification of macromolecular assemblies studied as 'single particles'. *Q. Rev. Biophys.* 23:281-329.

Funatsu, T., E. Kono, and S. Tsukita. 1993. Time-resolved electron microscopic analysis of the behavior of myosin heads on actin filaments after photolysis of caged ATP. *J. Cell Biol.* 121:1053-1064.

Goldman, Y. E. 1987. Kinetics of the actomyosin ATPase in muscle fibers. *Annu. Rev. Physiol.* 49:637-654.

Greenacre, M. J. 1993. Theory and applications of correspondence analysis. Academic Press, London. 1984.

Harauz, G., E. Boekema, and M. G. van Heel. 1988. Statistical image analysis of electron micrographs of ribosomal subunits. *Methods Enzymol.* 164: 35-49.

Harford, J. J., and J. M. Squire. 1992. Evidence for structurally different attached states of myosin cross-bridges on actin during contraction of fish muscle. *Biophys. J.* 63:387-396.

Haselgrove, J. C., and H. E. Huxley. 1973. X-ray evidence for radial cross-bridge movement and for the sliding filament model in actively contracting skeletal muscle. *J. Mol. Biol.* 77:549-568.

Haselgrove, J. C., M. Stewart, and H. E. Huxley. 1976. Cross-bridge movement during muscle contraction. *Nature (Lond.).* 261:606-608.

Henderson, R., J. M. Baldwin, K. H. Downing, J. Lepault, and K. Zemlin. 1986. Structure of purple membrane from *Halobacterium Halobium:* recording, measurement, and evaluation of electron micrographs at 3.5 A resolution. *Ultramicroscopy.* 19:147-178.

Heuser, J. E. 1983. Structure of the myosin crossbridge lattice in insect flight muscle. *J. Mol. Biol.* 169:123-154.

Heuser, J. E., T. S. Reese, M. J. Dennis, Y. Jan, L. Jan, and L. Evans. 1979. Synaptic vesicle exocytosis captured by quick freezing and correlated with quantal transmitter release. *J. Cell Biol.* 81:275-300.

Hirose, K., and T. Wakabayashi. 1993. Structural change of crossbridges of rabbit skeletal muscle during isometric contraction. *J. Muscle Res. Cell Motil.* 14:432-445.

Hirose, K., T. D. Lenart, J. M. Murray, C. Franzini-Armstrong, and Y. E. Goldman. 1993. Flash and smash: rapid freezing of muscle fibers activated by photolysis of caged ATP. *Biophys. J.* 65:397-408.

Holmes, K. C., D. Popp, W. Gebhard, and W. Kabsch. 1990. Atomic model of the actin filament. *Nature (Lond.).* 347:44-49.

Honda, H., Y. Koiwa, and N. Yagi. 1993. Myosin head movement of the rat slow skeletal-muscle as a function of calcium concentration. *J. Muscle Res. Cell Motil.* 14:364-365.

Hubert, L., and P. Arabie. 1985. Comparing partitions. *J. Classif.* 2:193-218.

Huxley, H. E. 1968. Structural difference between resting and rigor muscle; evidence from intensity changes in the low angle equatorial x-ray diagram. *J. Mol. Biol.* 37:507-520.

Huxley, H. E., and W. Brown. 1967. The low-angle x-ray diagram of vertebrate striated muscle and its behaviour during contraction and rigor. *J. Mol. Biol.* 30:383-434.

Huxley, H. E., and A. R. Faruqi. 1983. Time-resolved x-ray diffraction studies on vertebrate striated muscle. *Annu. Rev. Of Biophys. Bioeng.* 12:381-417.

Irving, T. C., and B. M. Millman. 1989. Changes in thick filament structure during compression of the filament lattice in relaxed frog sartorius muscle. *J. Muscle Res. Cell Motil.* 10:385-394.

Katayama, E. 1989. The effects of various nucleotides on the structure of actin-attached myosin subfragment-1 studied by quick-freeze deep-etch electron microscopy. *J. Biochem.* 106:751-770.

Lebart, L. 1994. Multivariate descriptive statistical analysis: correspondence analysis and related techniques for large matrices. John Wiley & Sons, Inc., New York. 231 pp.

Lenart, T. D., T. S. Allen, R. J. Barsotti, G. C. R. Ellis-Davies, J. H. Kaplan, C. Franzini-Armstrong, and Y. E. Goldman. 1993. Mechanics and structure of cross-bridges during contractions initiated by photolysis of caged Ca^{2+}. *In* Mechanism of myofilament sliding in muscle contraction. H. Sugi, editor. Plenum Publishing Corp., New York. 475-487.

Lepault, J., I. Erk, G. Nicolas, and J. L. Ranck. 1991. Time-resolved cryo-electron microscopy of vitrified muscular components. *J. Microsc. (Oxford)* 161:47-57.

Mezzich, J. E., and S. Solomon. 1980. Taxonomy and behavioral science: comparative performance of grouping methods. Academic Press, New York. 178 pp.

Milligan, R. A., and P. F. Flicker. 1987. Structural relationships of actin, myosin, and tropomyosin revealed by cryo-electron microscopy. *J. Cell Biol.* 105:29-39.

Milligan, R. A., M. Whittaker, and D. Safer. 1990. Molecular structure of F-actin and location of surface binding sites. *Nature (Lond.).* 348:217-221.

Ostap, E. M., H. D. White, and D. D. Thomas. 1993. Transient detection of spin-labeled myosin subfragment 1 conformational states during ATP hydrolysis. *Biochemistry.* 32:6712-6720.

Pollard, T. D., D. Bhandari, P. Maupin, D. Wachsstock, A. G. Weeds, and H. G. Zot. 1993. Direct visualization by electron microscopy of the weakly bound intermediates in the actomyosin adenosine triphosphatase cycle. *Biophys. J.* 64:454-471.

Poole, K. J., Y. Maeda, G. Rapp, and R. S. Goody. 1991. Dynamic x-ray diffraction measurements following photolytic relaxation and activation of skinned rabbit psoas fibres. *Adv. Biophys.* 27:63-75.

Rayment, I., and H. M. Holden. 1994. The 3-dimensional structure of a molecular motor. *Trends Biochem. Sci.* 19:129-134.

Rayment, I., H. M. Holden, M. Whittaker, C. B. Yohn, M. Lorenz, K. C. Holmes, and R. A. Milligan. 1993*a*. Structure of the actin-myosin complex

and its implications for muscle contraction. *Science (Wash. DC).* 261:58–65.
Rayment, I., W. R. Rypniewski, K. Schmidt-Base, R. Smith, D. R. Tomchick, M. M. Benning, D. A. Winkelmann, G. Wesenberg, and H. M. Holden. 1993*b*. 3-Dimensional structure of myosin subfragment-1: A molecular motor. *Science (Wash. DC).* 261:50–58.
Reedy, M. K., and M. C. Reedy. 1985. Rigor crossbridge structure in tilted single filament layers and flared-X formations from insect flight muscle. *J. Mol. Biol.* 185:145–176.
Reedy, M. C., M. K. Reedy, and R. T. Tregear. 1988. Two attached non-rigor crossbridge forms in insect flight muscle. *J. Mol. Biol.* 204:357–383.
Sosa, H., D. Popp, G. Ouyang, and H. E. Huxley. 1994. Ultrastructure of skeletal muscle fibers studied by a plunge quick freezing method: Myofilament lengths. *Biophys. J.* 67:283–292.
Squire, J. M., P. K. Luther, and E. P. Morris. 1990. Organisation and properties of the striated muscle sarcomere. *In* Molecular mechanisms in muscle contraction. J. M. Squire, editor. CRC Press, Boca Raton, FL. 1–48.
Stein, R. A., R. D. Ludescher, P. S. Dahlberg, P. G. Fajer, R. L. Bennett, and D. D. Thomas. 1990. Time-resolved rotational dynamics of phosphorescent-labeled myosin heads in contracting muscle fibers. *Biochemistry.* 29:10023–10031.
Sutoh, K., K. Yamamoto, and T. Wakabayashi. 1986. Electron microscopic visualization of the ATPase site of myosin by photoaffinity labeling with a biotinylated photoreactive ADP analog. *Proc. Natl. Acad. Sci. USA.* 83: 212–216.
Tanner, J. W., D. D. Thomas, and Y. E. Goldman. 1992. Transients in orientation of a fluorescent cross-bridge probe following photolysis of caged nucleotides in skeletal muscle fibres. *J. Mol. Biol.* 223:185–203.
Taylor, K. A., and L. A. Amos. 1981. A new model for the geometry of the binding of myosin crossbridges to muscle thin filaments. *J. Mol. Biol.* 147:297–324.
Taylor, K. A., M. C. Reedy, L. Cordova, and M. K. Reedy. 1984. Three-dimensional reconstruction of rigor insect flight muscle from tilted thin sections. *Nature (Lond.).* 310:285–291.
Taylor, K. A., M. C. Reedy, L. Cordova, and M. K. Reedy. 1986. Image reconstruction using electron micrographs of insect flight muscle. Use of thick transverse sections to supplement data from tilted thin longitudinal sections. *Biophys. J.* 49:353–364.
Taylor, K. A., M. C. Reedy, L. Cordova, and M. K. Reedy. 1989. Three-dimensional image reconstruction of insect flight muscle. I. The rigor myac layer. *J. Cell Biol.* 109:1085–1102.
Tokunaga, M., K. Sutoh, C. Toyoshima, and T. Wakabayashi. 1987. Location of the ATPase site of myosin determined by three-dimensional electron microscopy. *Nature (Lond.).* 329:635–638.
Toyoshima, C., and T. Wakabayashi. 1985*a*. Three-dimensional image analysis of the complex of thin filaments and myosin molecules from skeletal muscle. V. Assignment of actin in the actin-tropomyosin-myosin subfragment-1 complex. *J. Biochem. (Tokyo).* 97: 245–263.
Toyoshima, C., and T. Wakabayashi. 1985*b*. Three-dimensional image analysis of the complex of thin filaments and myosin molecules from skeletal muscle. IV. Reconstitution from minimal- and high-dose images of the actin-tropomyosin-myosin subfragment-1 complex. *J. Biochem. (Tokyo).* 97: 219–243.
Trus, B. L., A. C. Steven, A. W. McDowall, M. Unser, J. Dubochet, and R. J. Podolsky. 1989. Interactions between actin and myosin filaments in skeletal muscle visualized in frozen-hydrated thin sections. *Biophys. J.* 55:713–724.
Tsukita, S., and M. Yano. 1985. Actomyosin structure in contracting muscle detected by rapid freezing. *Nature (Lond.).* 317:182–184.
Unser, M., and M. Eden. 1990. Weighted averaging of a set of noisy images for maximum signal-to-noise ratio. *IEEE (Inst. Electr. Electron. Eng.) Trans. Acoustics Speech Signal Process.* 38:890–895.
Unser, M., B. L. Trus, and A. C. Steven. 1989. Normalization procedures and factorial representations for classification of correlation-aligned images: a comparative study. *Ultramicroscopy.* 30:299–310.
van Heel, M. G. 1984. Multivariate statistical classification of noisy images (randomly oriented biological macromolecules). *Ultramicroscopy.* 13: 165–183.
Varriano-Marston, E., C. Franzini-Armstrong, and J. C. Haselgrove. 1984. The structure and disposition of crossbridges in deep-etched fish muscle. *J. Muscle Res. Cell Motil.* 5:363–386.
Vibert, P., and R. Craig. 1982. Three-dimensional reconstruction of thin filaments decorated with a Ca^{2+}-regulated myosin. *J. Mol. Biol.* 157:299–319.
Walker, M., H. D. White, B. Belknap, and J. Trinick. 1994. Electron cryomicroscopy of acto-myosin-S1 during steady-state ATP hydrolysis. *Biophys. J.* 66:1563–1572.
Ward, J. H., Jr. 1963. Hierarchical grouping to optimize an objective function. *J. Am. Stat. Assoc.* 58:236–244.
Winkelmann, D. A., T. S. Baker, and I. Rayment. 1991. Three-dimensional structure of myosin subfragment-1 from electron microscopy of sectioned crystals. *J. Cell Biol.* 114:701–713.
Yount, R. G., C. R. Cremo, J. C. Grammer, and B. A. Kerwin. 1992. Photochemical mapping of the active site of myosin. *Philos. Trans. R. Soc. Lond. B. Biol. Sci.* 336:55–60.
Yu, L. C., and B. Brenner. 1989. Structures of actomyosin crossbridges in relaxed and rigor muscle fibers. *Biophys. J.* 55:441–453.
Yu, L. C., A. C. Steven, G. R. Naylor, R. C. Gamble, and R. J. Podolsky. 1985. Distribution of mass in relaxed frog skeletal muscle and its redistribution upon activation. *Biophys. J.* 47:311–321.